Nano Energy (2016) 19, 27–38

Available online at www.sciencedirect.com

ScienceDirect

journal homepage: www.elsevier.com/locate/nanoenergy

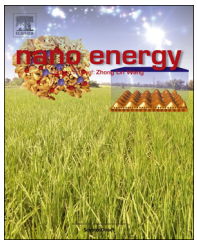

RAPID COMMUNICATION

Optimization of sulfur-doped graphene as an emerging platinum nanowires support for oxygen reduction reaction

Md. Ariful Hoque[a], Fathy M. Hassan[a], Min-Ho Seo[a], Ja-Yeon Choi[a], Mark Pritzker[a], Shanna Knights[b], Siyu Ye[b], Zhongwei Chen[a,*]

[a]*Department of Chemical Engineering, Waterloo Institute for Nanotechnology, Waterloo Institute of Sustainable Energy, University of Waterloo, 200 University Ave. W, Waterloo, ON, Canada N2L 3G1*
[b]*Ballard Power Systems, Inc., 9000 Glenlyon Parkway, Burnaby, BC, Canada V5J 5J8*

Received 8 July 2015; received in revised form 6 November 2015; accepted 9 November 2015
Available online 17 November 2015

KEYWORDS
S doped graphene;
S contents;
Pt nanowires;
Oxygen reduction;
Activation energy

Abstract
The slow kinetics of the oxygen reduction reaction (ORR) on platinum catalyst is a critical parameter for application in polymer electrolyte membrane fuel cells (PEMFCs). Herein, we study the effects of sulfur on the electrochemical activity and stability of sulfur doped graphene supported platinum nanowires (PtNW/SGs). To investigate the influence of sulfur, a series of sulfur-doped graphene materials with varying sulfur contents ranging from 0.35 to 3.95 at% are applied as platinum nanowire catalyst supports. Based on the physico-chemical characterizations, electrochemical measurements and density functional theory (DFT) calculations, we find that the amount of sulfur significantly affects the electrokinetics of the Pt nanowires. The best ORR kinetics are observed for the platinum nanowires supported on graphene with 1.40 at% sulfur, showing a mass activity of 182 mA/mg_{Pt} and a specific activity of 662 μA/cm^2_{Pt} at 0.9 V vs. RHE. At this sulfur content, well-defined platinum nanowires with diameters in the range of 4–16 nm are observed that are beneficial for enhancing ORR kinetics.

Introduction

The kinetic limitations of the cathodic oxygen reduction reaction (ORR) must be overcome to meet the practical demands for polymer electrolyte membrane fuel cells

*Corresponding author.
E-mail address: zhwchen@uwaterloo.ca (Z. Chen).

http://dx.doi.org/10.1016/j.nanoen.2015.11.004
2211-2855/

(PEMFCs) [1-5]. The observed overpotential is attributed to the slow kinetics of ORR occurring on the conventional carbon supported platinum nanoparticle (Pt/C) catalysts [6-8]. These zero dimensional (0D) nanoparticulate electrocatalysts lack activity due to a high number of defect sites, lattice boundaries and low coordination atoms on the surface that results from their very small size. This leads to the strong adsorption of oxygen containing species (i.e., OH groups) and thereby decreases the number of active platinum sites available for the ORR [9-12]. Stability is another pertinent concern, whereby Pt/C degrades during PEMFC operation due to carbon corrosion and/or platinum nanoparticles agglomeration, dissolution and Ostwald ripening [13-15].

In contrast to nanoparticles, one dimensional (1D) nanostructures, such as platinum nanowires, have been highly touted as promising solutions to the inherent activity and durability issues associated with state-of-the-art nanoparticle catalysts [16-21]. These 1D platinum morphologies provide significant advantages owing to their unique anisotropic structure and surface properties that lead to excellent electrocatalytic activity and durability [9,22,23]. In particular, platinum nanowire morphologies minimize the number of undesirable low-coordination defect sites due to their preferential exposure of smooth crystalline planes [24-26]. Therefore, the cathodic overpotential caused by adsorbed oxygen-containing species can be significantly suppressed, leading to an increase in ORR kinetics [27,28].

The performance of platinum nanoparticles or nanowires can be further improved by growing them onto a variety of stable supports, including mesoporous carbon, carbon nanofibers, carbon nanotubes and graphene [29-36]. Among these supports, graphene has significant application potential owing to its unique properties [37]. The two dimensional sp^2 bonded hybridized carbon network in particular possesses outstanding mechanical, chemical and electrical properties that are ideal for electrochemical applications [38]. Both theoretical calculations and detailed experiments have shown that the intrinsic properties of graphene can be modified by the introduction of heteroatoms, such as sulfur, nitrogen, phosphorus or boron into the carbon frameworks [32,39-41]. A lot of research has been carried out to investigate nitrogen doped carbon materials as platinum catalyst supports, with enhancements to both ORR activity and electrochemical stability observed [42-46]. We were however the first to develop sulfur-doped graphene (SG) as a platinum catalyst support, capable of providing remarkable activity and durability improvements [32,33]. Through detailed density functional theory (DFT) calculations and experimental investigations, we demonstrated that platinum binds strongly to SG. These strong catalyst-support interactions lead to an enhancement in Pt stabilization, along with modulated electronic properties that provide ORR activity enhancements. The amount of sulfur in SG very likely has a significant impact on the interactions with platinum, owing to its influence on the electrical and chemical properties of the resulting catalyst. Therefore, detailed knowledge of the sulfur concentration dependency of the electro-kinetic parameters for oxygen reduction, along with the physichochemical properties of the developed catalysts is of importance. This fundamental insight is essential to the design and development of optimal Pt-SG catalysts.

In this report, we provide an extensive investigation to elucidate the effect of sulfur concentration on the oxygen reduction performance of SG supported platinum nanowires (PtNW/SG). We examine the morphologies, structural and electrical properties of PtNW/SG with different sulfur contents, and then investigated the electrochemical kinetic parameters such as Tafel slope, exchange current density and activation energy towards oxygen reduction. These detailed experimental investigations are also linked to computational simulations to systematically elucidate the impact and contribution of sulfur on the ORR activity of PtNW catalysts.

Experimental section

Synthesis of graphene oxide (GO)

Graphite powder (Alfa Aesar, natural, microcrystal grade, APS 2-15 micron, 99.9995%) was oxidized by an improved Hummers method in order to obtain GO [47]. Briefly, 2 g of graphite powder was added to a mixture of concentrated H_2SO_4/H_3PO_4 (360:40 mL) in a triangular shaped conical flask. After 30 min of magnetic stirring, 18 g of $KMnO_4$ was added very slowly and the reaction was heated to 50 °C and held for 16 h. Once the reaction was completed, the temperature was cooled down to ca. 10 °C in an ice container and then 400 mL of DDI H_2O was added in a dropwise fashion. 15 mL of H_2O_2 (30%) was then added to complete the oxidation reaction. The final mixture was centrifuged and washed with water, ethanol and HCl (30%), and then freeze dried for 3-4 days.

Synthesis of SG and G

Graphene with different sulfur concentrations was prepared by a thermal shock/quench annealing process. Briefly, 120 mg of GO and the desired amount of phenyl disulfide (PDS, Sigma Aldrich) were mixed together by grinding. Different sulfur contents were achieved by adding 10, 60, 240 and 480 mg of PDS to the mixture. This mixture was then transferred into a quartz tube for annealing at 1000 °C for 30 min under Ar atmosphere [32]. This was accomplished by keeping the sample upstream (out of the heating zone) while the furnace reached the desired temperature, at which point it was inserted into the heating zone. After the desired reaction time, the sample was removed from the heating zone so that it would cool rapidly. Pure graphene was also synthesized by directly annealing GO under the same conditions.

Synthesis of PtNW/SG and PtNW/G

To grow platinum nanowires onto the SG, 20 mg of SG was first dispersed by ultrasonication for at least 2 h in a mixture of 4 mL ethylene glycol (EG) and 6 mL of N,N-dimethyl formaide (DMF). 53 mg of $H_2PtCl_6 \cdot 6H_2O$ was then added to the solution, followed by the addition of 0.5 g KOH. The resultant solution was magnetically stirred overnight and then transferred into a 20 mL Teflon-lined autoclave to heat in a convection oven at 170 °C for 8 h. The final material was collected for thorough washing with ethanol and DDI water before drying in a vacuum oven at 80 °C. Using this method,

the same Pt loading (50 wt%) was achieved onto the various SG supports. The same procedure was applied to prepare platinum nanowires supported on pure graphene (PtNW/G).

Material characterization

The samples were characterized by Transmission Electron Microscopy (TEM, Zeiss Libra 200 MC) equipped with EDX for elemental mapping, Raman spectroscopy (SENTERRA 314), XRD (Inel XRG 3000 diffractometer), X-ray photoelectron spectroscopy (XPS, PHI Quantera) and Scanning Electron Microscopy (SEM, LEO FESEM 1530) equipped with EDX. The optical properties of the prepared SG samples were analyzed by UV-visible spectroscopy (Ocean Optics, DT-MINI-2-GS). Linear polarization (LPR) was carried out on a 2-point probe system to obtain the electrical conductivity of G, SGs and GO prepared under different conditions [48].

Electrochemical characterization

To conduct electrochemical testing of the catalyst materials, the electrode was prepared by dispersing 2 mg of catalyst materials in a solution containing 0.95 mL ethanol and 0.05 mL 5% Nafion. The electrode loading of the different nanowire catalysts and the commercial state-of-the-art Pt/C (TKK, 28.2 wt% Pt) was controlled to be 22 $\mu gPt/cm^2$. Cyclic voltammetry (CV) curves were collected at a scan rate of 50 mV/s in N_2-saturated 0.1 M $HClO_4$ and the ORR measurements were conducted at a scan rate of 5 mV/s in O_2-saturated 0.1M $HClO_4$ at room temperature. Accelerated durability testing (ADT) was performed by cycling the electrode potential 1000 times in a N_2-saturated electrolyte between 0.05 and 1.5 V vs. RHE at a scan rate of 50 mV/s. The temperature dependent kinetic parameters for ORR on oxide-covered and oxide-free platinum surfaces of the different catalysts were calculated at atmospheric pressure. Throughout the electrochemical investigations, the temperature was varied from 20 to 50 °C using a waterbath (Polystar®-Cole Polymer®) and the cell temperature was initially maintained at 20 °C for at least 2 h in order to ensure thermal equilibration [49]. A potential scan between 0.05 and 1.5 V vs. RHE at a scan rate of 50 mV/s in O_2-saturated 0.1 M $HClO_4$ was applied during the equilibration period to maintain the electrode in an activated state. Then, slow scan voltamograms for oxygen reduction were collected by sweeping the potential from 0.3 to 1.2 V vs. RHE at scan rate of 1 mV/s [50]. In this way, all the kinetic parameters were calculated at each temperature. Moreover, the temperature was subsequently lowered back to check for hysteresis. It should be noted that all of the results were electrolyte resistance corrected [51]. 20 wt% carbon black (Vulcan XC-720) was added to the suspension in order to improve the dispersion of the nanowire catalyst on the glassy carbon electrode.

Results and discussion

Physico-chemical characterization

Figure 1a depicts a TEM image that represents the general graphene morphology of all SG materials. An EDX elemental map was carried out on each sample and the distribution of

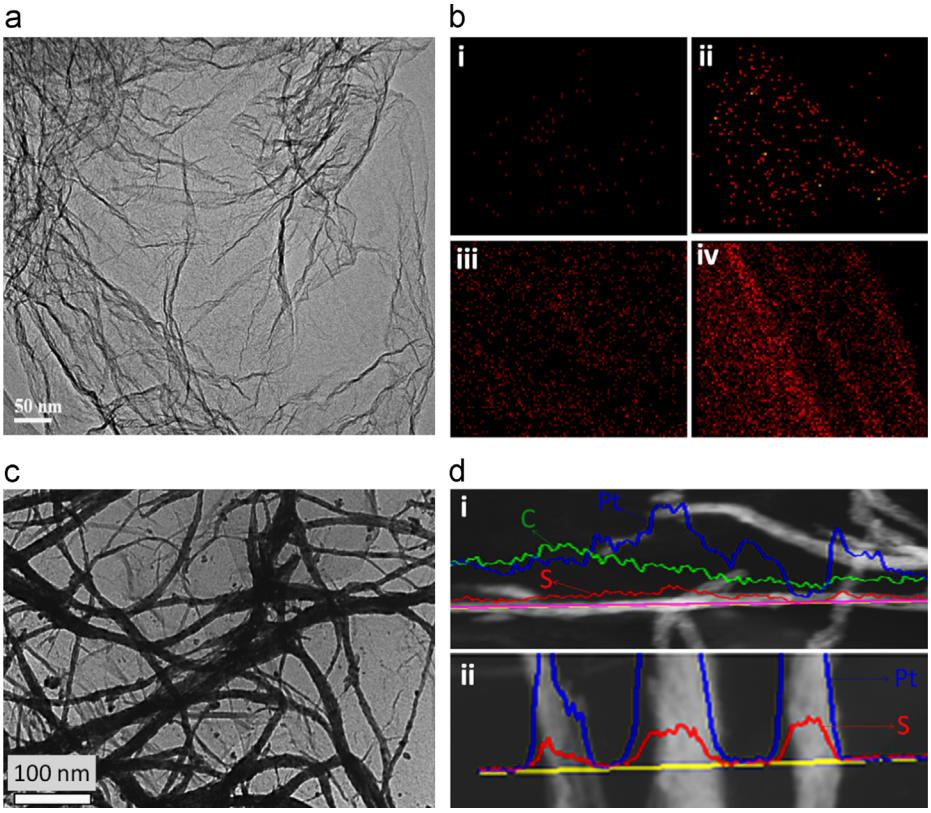

Figure 1 (a) TEM image of SG, (b) elemental color maps for sulfur corresponds to (i) SG-1, (ii) SG-2, (iii) SG-3 and (iv) SG-4. (c) TEM image of PtNW on SG-2 and (d) EDX line scans along both (i) the length and (ii) the cross section of the nanowires.

sulfur species were depicted in Figure 1b (i-iv). It was observed that sulfur atoms are well distributed and the amount of sulfur increases with increased amounts of PDS added during synthesis. Using both EDX and XPS (Table S1 in Supporting information), the sulfur contents of SG were 0.35, 1.40, 2.70 and 3.95 at%, corresponding to the addition of 10, 60, 240 and 480 mg of PDS during synthesis, respectively. These materials are named in order of increasing sulfur content as SG-1, SG-2, SG-3 and SG-4. The morphologies of the PtNW after deposition on SG-2 were investigated using TEM as shown in Figure 1c. The diameter of the nanowires was in the range of 3–30 nm, along with nanowire lengths in excess of 1 μm. We conducted elemental line scans to locate carbon, sulfur and platinum species along both the length and cross section of the nanowires, shown in Figure 1d (i-ii). Interestingly, the composition profile of the sulfur atoms closely matched that of platinum. One may consider that this is due to the presence of free sulfur species "poisoning" the surface of the platinum nanowires, owing to the affinity between these two atoms. To exclude this, EDX spectra were collected from a PtNW that extends beyond the surface of the underlying SG-2 support. No sulfur was detected during this scan, suggesting that the similar composition profile of sulfur and platinum is due to the sulfur species within SG acts as anchoring sites for the PtNWs. In our previous studies [33] it was shown that the Pt nanowires grow directly onto SG, and are comprised of numerous single crystalline nanoparticles oriented along the ⟨111⟩ direction. TEM images and the corresponding cross sectional diameter distribution of the nanowires obtained by PtNW/G, PtNW/SG-1, PtNW/SG-2, PtNW/SG-3 and PtNW/SG-4 are shown in Figure S1-5 (See Supporting information). Interestingly, a major portion of nanowires having small sized diameter was observed for PtNW/SG-2 in comparison to other catalysts. For example, the distribution of diameter of the nanowires was dominant in the range of 8–23 nm for PtNW/G (Figure S1), 8–18 nm for PtNW/SG-1 (Figure S2), and 4–16 nm for PtNW/SG-2 (Figure S3). However, PtNW/SG-3 possess relatively larger diameters, (i.e., 20 nm) along with some nanoparticles agglomerated in an elongated structure (Figure S4) that we have previously shown as one of the steps of platinum nanowire growth [33]. On the other hand, the formation of nanowires was significantly interrupted in the case of PtNW/SG-4 and a high proportion of these elongated nanoparticle agglomerates was observed (Figure S5). XRD was used to confirm that all of these structures were in fact fcc phase platinum (Figure S6).

The nature of chemical bonding in SG was investigated by XPS. Figure 2a-d shows the characteristic C 1s peak obtained for the various SG materials. The typical C 1s region was deconvoluted into different envelopes, corresponding to the following bonds: sp^2 C=C (284.5 eV), sp^3 C-C (285.1 eV), C-O (286.2 eV), C=O (287.2), O-C-O (288.9 eV) and Π-Π^* transitions in delocalized sp^2 bonded carbon structures (>290 eV) [52]. These peak deconvolutions allowed for measurement of the ratio of sp^2 to sp^3 bonded carbon contents [52-55] with the values of 2.05, 1.86, 1.45 and 1.1 for SG-1, SG-2, SG-3 and SG-4 respectively. It is

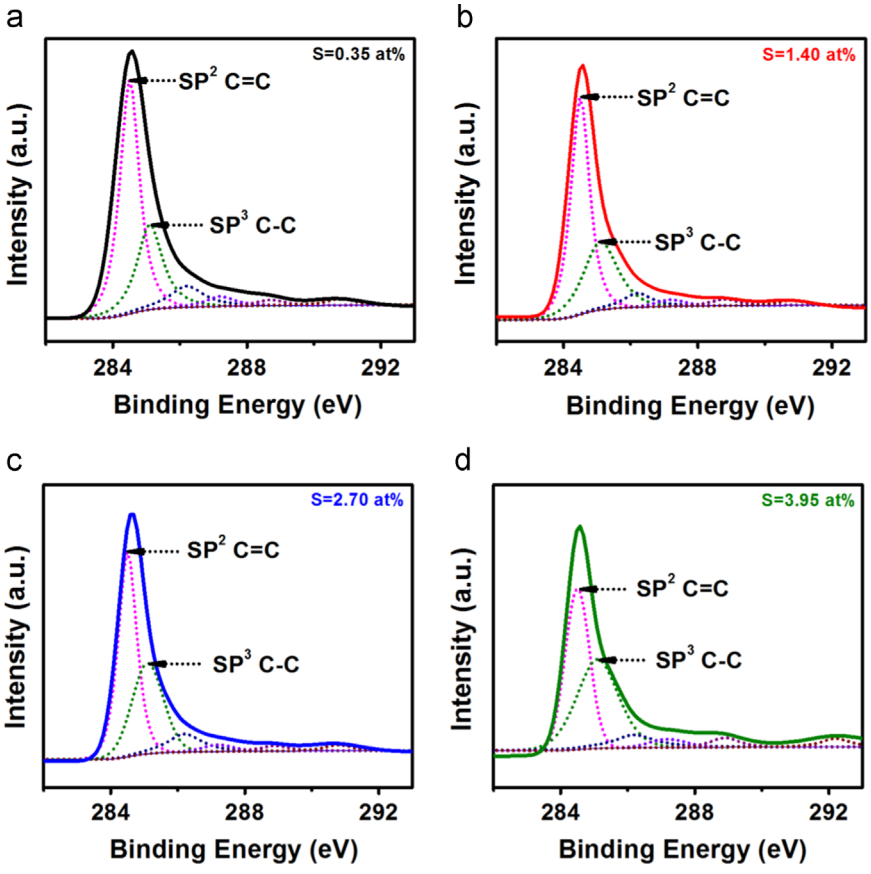

Figure 2 XPS high resolution C1s scan spectra for SG materials (a) SG-1, (b) SG-2, (c) SG-3 and (d) SG-4.

interesting to note that the concentration ratio of sp^2:sp^3 carbon decreases significantly with increasing sulfur contents in SG. This is to be expected, as the content of dopant species is commonly linked to decreased degrees of graphitization [56,57]. In reality, a fraction of edge/defect sites always exist in the graphene and with increasing amount of Phenyl disulfide (PDS) during synthesis, those fractions can be affected significantly that leads to higher amounts of sp^3 bonded carbon. Also, the S 2p XPS spectra for SG-1, SG-2, SG-3 and SG-4 are shown in Figure S7a (see Supporting information). The peaks observed at 163.8 and 165.1 eV suggest the presence of thiophenic sulfur dopants, whereas the peaks above 165.5 eV are assigned to -C-SO_x- species [36,58]. In addition with S peak analysis, the fitted Pt $4f_{7/2}$ and $4f_{5/2}$ peaks at 71.6 and 75.2 eV, respectively, for PtNW/SG-1, PtNW/SG-2, PtNW/SG-3 and PtNW/SG-4 are also shown in Figure S7b (see Supporting information). It should be noted that no significant structural changes were observed in the S and Pt spectra of the different SG samples, in contrast to the noticeable changes in the carbon bonding configuration.

The structure of the different SG supports was analyzed by XRD, with results shown in Figure 3a. The average interlayer spacing corresponding to the (002) peak at ca. 25° were 3.55, 3.49, 3.47, 3.41 and 3.38 Å for G, SG-1, SG-2, SG-3 and SG-4, respectively. It is clear that the d spacing values of various SG supports decrease with an increase in sulfur content. This is likely due to the fact that more oxygen functional species are removed with increasing amounts of sulfur [59]. In particular, the oxygen content of SG was found to decrease from 12.9 at% for SG-1 to 2.3 at% for SG-4 (Table S1 in Supporting information). In addition, the thickness of the graphene platelets can be determined by calculating the crystallite sizes (Lc) in the (002) direction using the Scherrer equation:

$$Lc = A\lambda/B\cos\theta$$

where A is the shape factor ($\sim$0.9), λ is the X-ray wave length, θ is the Bragg angle and B is the full width at half maximum (FWHM) of the (002) peak in radians. The crystallite size, Lc increases with an increase in sulfur concentration, with thicknesses of 13.5, 18.1, 20.0, 35.1 and 43.8 Å for G, SG-1, SG-2, SG-3 and SG-4, respectively. The number of graphene layers can then be estimated [60,61] by correlating Lc with the corresponding d spacing values to be 3.8, 5.4, 6.2, 10.3 and 13.1, for G, SG-1, SG-2, SG-3 and SG-4, respectively. The d spacing and the number of layers were increased significantly for SG-3 and SG-4, which indicate that a high loading of sulfur precursor may enhance the restacking of graphene layers. This likely occurs due to increased removal of oxygen species that was found concurrently with higher sulfur contents.

Raman was used as a quantitative measure to estimate the degree of disorder in SG with different sulfur concentrations and results are shown in Figure 3b. In the spectra, the ratio of the D band intensity to the G band intensity (I_D/I_G) were ca. 1.10, 1.23, 1.35 and 1.43 for SG-1, SG-2, SG-3 and SG-4, respectively. All of these values for SG materials were higher than that of un-doped G (I_D/I_G: 0.96). This shows that the sulfur atoms present in SG are in the form of defects. This is to be expected considering that XPS indicated sulfur atoms are present in thiophenic form, which is a five ring structure that disrupts the crystalline planes of graphene.

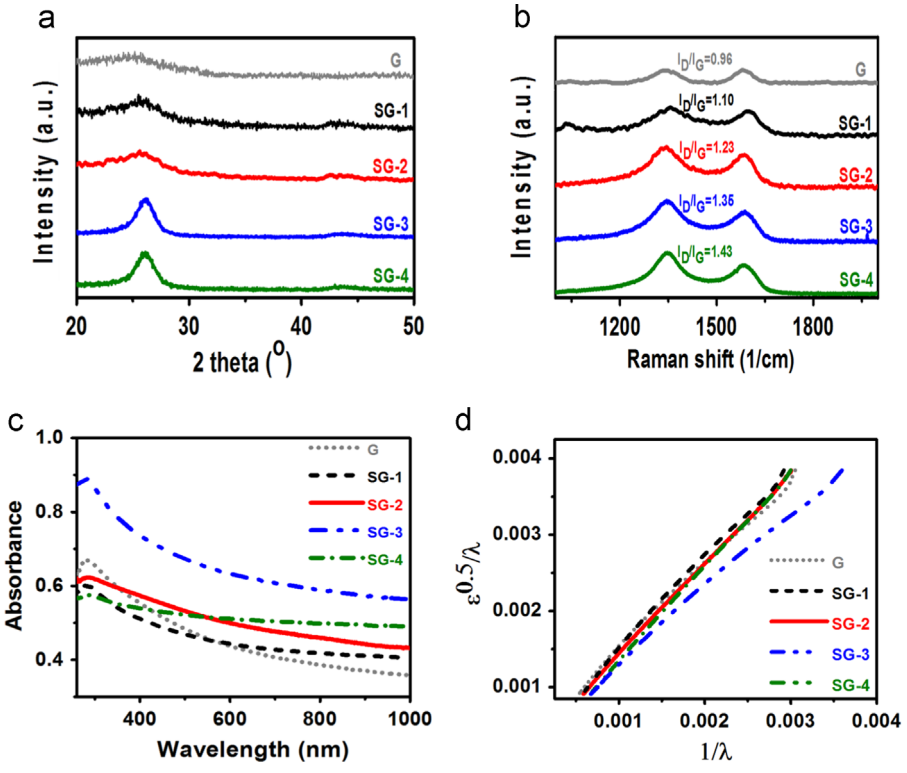

Figure 3 (a) XRD for G and SG materials, (b) Raman spectroscopy of G and SG materials, (c) UV absorption data for G and SG materials, and (d) Band-gap curves of G and SG materials.

Figure 3c shows the UV-vis absorption spectra of G, SG-1, SG-2, SG-3, SG-4 with a peak centered at 268 nm. To determine the energy band gap (E_g), Tauc's equation was applied [62]:

$$\omega^2\epsilon = (h\omega - E_g)^2$$

where ε is the absorbance, ω is the angular frequency of light which is $2\sqcap/\lambda$, h is the Planck constant and λ is the wavelength. On plotting $\varepsilon^{1/2}/\lambda$ vs. $1/\lambda$ (Figure 3d), a straight line intersecting with the x-axis is $1/\lambda g$ (λg is the gap wave length) [63-65]. The energy band gap was calculated based on $E_g = hc/\lambda g$ to be 0.45, 0.54, 0.61, 0.72 and 0.84 eV for of G, SG-1, SG-2, SG-3 and SG-4 respectively. It should be noted that the band gap increases in the order of SG-4 > SG-3 > SG-2 > SG-1 > G, suggesting a decrease in intrinsic conductivity due to an increasing amount of sulfur in graphene. The trend observed is likely due to the lower graphitic character of the SG materials with increased sulfur concentrations, confirmed both by XPS and Raman spectroscopy. The intrinsic conductivity of G and various SGs was in fact measured using the 2-point probe method [48] and the results obtained from the LPR technique are shown in Figure S8 in the Supporting information. The following equation was applied to measure the intrinsic conductivity of the materials.

$$\sigma = L/RA$$

where σ is the conductivity in S/cm, L is the thickness of the electrode in cm, R is the resistance in Ω and A is the cross sectional area of electrode in cm^2. From the LPR technique applied, the resistance decreases in the order of GO > SG-4 > SG-3 > SG-2 > SG-1 > G. Therefore, the intrinsic conductivities determined for G, SG-1, SG-2, SG-3, SG-4 and GO were 16.5, 13.9, 10.6, 7.3, 1.6 and 1.4×10^{-4} S/cm, respectively, values that are within the range of previously reported results from the literature [66]. EIS results in Figure S9 in the Supporting information show that G has lower interfacial electron transfer resistance, R_{et} than SG-2 which is consistent with the results obtained by LPR and UV-vis analysis. The trends clearly show that the electrical conductivity of SG decreases with an increasing sulfur content. Despite the fact that conductivity plays an important role in electrocatalysis, the best ORR performance was achieved for PtNW/SG-2 with a sulfur content of 1.40 at% (vide infra). This suggests that at this content, conductivity limitations do not present a significant issue.

Electrochemical characterization

Cyclic voltammetry (CV) was used to investigate the effect of sulfur concentration on the electrochemical properties of the PtNW/G and PtNW/SG. Figure 4a shows the steady state CVs of PtNW/G, PtNW/SG-1, PtNW/SG-2, PtNW/SG-3 and PtNW/SG-4 obtained in N_2-saturated 0.1 M $HClO_4$ solution. The typical hydrogen adsorption/desorption signature is observed in the 0.05-0.4 V vs. RHE potential range. Electrochemical double layer capacitance is observed between 0.4 and 0.7 V vs. RHE, and platinum oxidation/reduction occur in the range of 0.7-0.9 V vs. RHE. ECSA values were determined based on the calculated charge for hydrogen adsorption/desorption of each voltamogram using the following equation [67,68]:

$$\mathrm{ECSA} = Q \,/\, (0.21 * L)$$

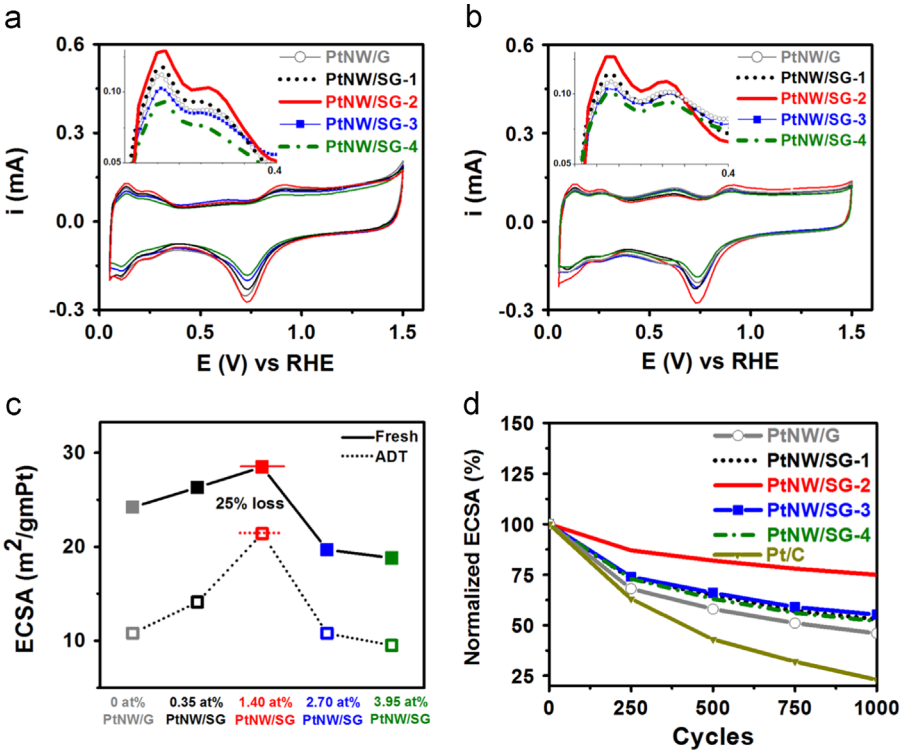

Figure 4 Electrochemical evaluation. CV curves (a) initially and (b) after ADT obtained for PtNW/G, PtNW/SG-1, PtNW/SG-2, PtNW/SG-3 and PtNW/SG-4, (c) Comparison of ECSA of each catalyst before and after ADT and (d) Normalized ECSA remaining throughout ADT.

where, Q indicates the charge density for hydrogen adsorption (mC/cm^2) that can be calculated by integrating the hydrogen adsorption/desorption region and dividing by the potential scan rate, L is the mass loading of Pt on the electrode (mg/cm^2) and the factor 0.21 (mC/cm^2_{Pt}) is due to the charge required to reduce a monolayer of protons on Pt. The ECSA values determined for PtNW/G, PtNW/SG-1, PtNW/SG-2, PtNW/SG-3 and PtNW/SG-4 are 24.2, 26.3, 28.5, 19.7 and 18.8 $m^2/g_{Pt,}$ respectively. Figure 4b shows the CV curves obtained for various catalyst materials subjected to 1000 potential cycles between 0.05 and 1.5 V vs. RHE. After ADT, the ECSA values calculated for PtNW/G, PtNW/SG-1, PtNW/SG-2, PtNW/SG-3 and PtNW/SG-4 are 10.8, 14.1, 21.4, 10.8 and 9.5 $m^2/g_{Pt,}$ respectively. However, ECSA values obtained for Pt/C before and after ADT are 54.5 and 13.1 m2/gpt, respectively (Figure S10 in the Supporting information). The reduced ECSA of the nanowire catalysts in comparison to Pt/C is expected due to the thicker diameter and anisotropic structure that results in a lower degree of Pt-atom exposure [13,23]. A comparison of the ECSA values of various catalysts has been shown in Figure 4c. Normalized ECSA values obtained initially and after each 250 subsequent cycles are shown in Figure 4d. It can be seen that the ECSA retention of PtNW/SG-2 is higher, retaining 75% of its initial surface area whereas the retention was 45, 53, 55, 51 and 24% for PtNW/G, PtNWSG-1, PtNW/SG-3, PtNW/SG-4 and Pt/C, respectively. The least ECSA retention exhibited by Pt/C in comparison to the nanowire catalysts can be explained by the TEM images and the particle size distribution shown in Figure S11 (See Supporting information). It can be seen that the nanoparticles are significantly affected and the average size is increased from 2.15 to 7.5 nm. These results indicate that PtNW/SG-2 has the highest electrochemical stability in terms of ECSA retention during potential cycling. Additionally, it was found that regardless of sulfur content, SG supported PtNWs demonstrated increased electrochemical stability in comparison to PtNW/G, reasserting the beneficial impact of sulfur species in the catalyst supports.

ORR measurements were carried out in O_2-saturated 0.1 M $HClO_4$ solution using a GC rotating disc electrode at room temperature in order to investigate the influence of sulfur on ORR activity of different nanowire catalysts. The polarization curves shown in Figure 5a and b display the diffusing-limiting current region from ca. 0.05 to 0.65 V vs. RHE and mixed kinetic-diffusion control region between ca. 0.7 and 1.05 V vs. RHE. All polarization plots were collected using identical platinum loadings on the electrode. It is clear that the half-wave potential of PtNW/SG-2 before and after ADT was higher than the other catalysts, indicating in addition to improved electrochemical durability, PtNW/SG-2 also provides improved ORR activity. After ADT, the half wave potential loss was only 15 mV for PtNW/SG-2. On the other hand, the losses in half-wave potential were 48, 40, 38, 45 and 56 mV for PtNW/G, PtNW/SG-1, PtNW/SG-3, PtNW/SG-4 and Pt/C, respectively (Figure 5c). To compare the mass activity of the different catalysts, kinetic current densities were calculated from the polarization curves by correcting for mass transport and then normalizing with respect to platinum loading [9,69]. The following Koutecky-Levich equation was applied to calculate the kinetic current density, j_k:

$$1/j = 1/j_k + 1/j_d$$

where j is the measured current density, j_k is the kinetic current density and j_d is the diffusion-limiting current

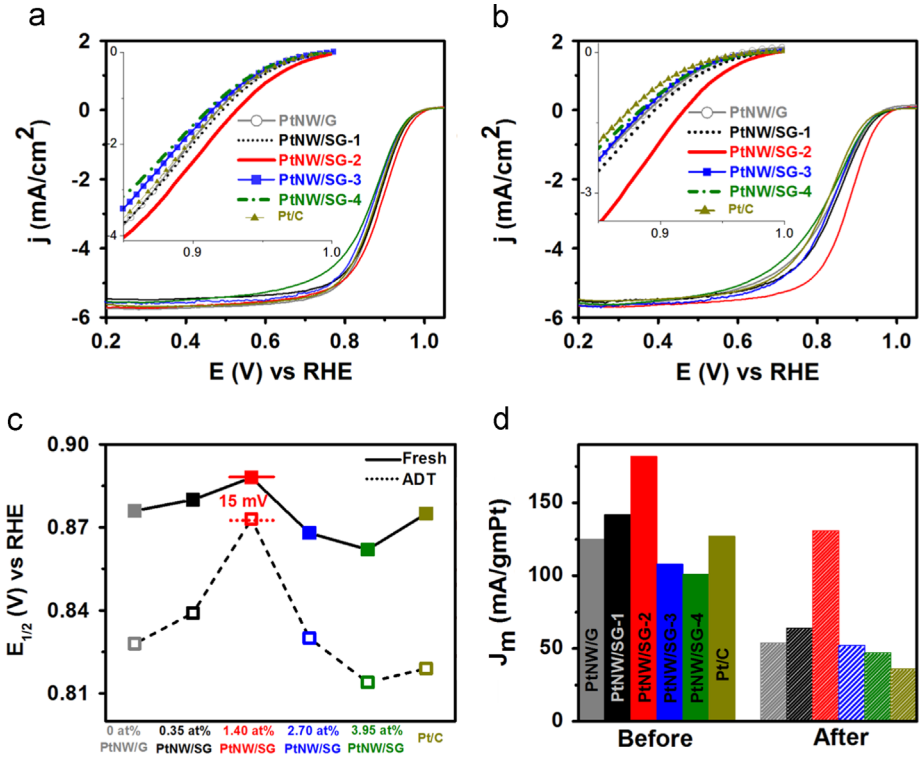

Figure 5 ORR polarization curves (a) initially and (b) after ADT obtained for PtNW/G, PtNW/SG-1, PtNW/SG-2, PtNW/SG-3, PtNW/SG-4 and Pt/C, (c) comparison of half-wave potential of each catalyst before and after ADT, and (d) kinetically corrected Pt mass based activities of each catalyst before and after ADT.

density. From Figure 5d, it can be seen that the initial mass activity calculated at 0.9 V vs. RHE for PtNW/SG-2 was 182 mA/mg_{Pt}, demonstrating excellent ORR activity in comparison with PtNW/G (125 mA/mg_{Pt}), PtNW/SG-1 (142 mA/mg_{Pt}), PtNW/SG-3 (108 mA/mg_{Pt}), PtNW/SG-4 (101 mA/mg_{Pt}) and Pt/C (127 mA/mg_{Pt}). After ADT, PtNW/SG-2 also demonstrated superior ORR stability, providing a mass activity of 131 mA/mg_{Pt} at 0.9 V vs. RHE, that represents 72% of its initial activity. Conversely, the mass activity retention after ADT for PtNW/G, PtNW/SG-1, PtNW/SG-3, PtNW/SG-4 and Pt/C were 43, 45, 48, 46 and 28%, respectively. Moreover, the specific activity determined at 0.9 V vs. RHE shown in Figure S12 (see Supporting information) for PtNW/SG-2 was higher (662 μA/cm^2_{Pt}) in comparison to PtNW/G (530 μA/cm^2_{Pt}), PtNW/SG-1 (556 μA/cm^2_{Pt}), PtNW/SG-3 (567 μA/cm^2_{Pt}), PtNW/SG-4 (542 μA/cm^2_{Pt}) and Pt/C (244 μA/cm^2_{Pt}), respectively. These results clearly indicate that SG-2 can effectively increase the activity of PtNW/SG-2. Notably, the Pt mass and specific activity obtained by PtNW/SG-2 was higher than some other results reported in the literature. These include carbon supported multiarmed starlike platinum nanowires that shows a mass activity of 135 mA/mg_{Pt} and a specific activity of 611 μA/cm^2_{Pt}, ultrathin Pt multiple-twinned nanowire networks that shows a mass activity of 144 mA/mg_{Pt} and a specific activity of 139 μA/cm^2_{Pt}, platinum nanocrystal supported by reduced graphene oxide that shows a mass activity of 109 mA/mg_{Pt} and a specific activity of 212 μA/cm^2_{Pt}, and Pt-Pd bimetallic nanodendrites that shows a mass activity of 204 mA/mg_{Pt} and a specific activity of 422 μA/cm^2_{Pt} [13,69-71]. It has been well established that ORR activity of Pt nanostructures increases accordingly with an appropriate decrease in the binding energy of oxygenated species to the Pt surface [72-75]. This is because low coordination surface Pt atoms of nanoparticle structures that are prone to block the active sites by oxygenated species, i.e. OH_{ads} inducing higher binding energy than the optimal values (~0.2 eV) [74,76]. However, Pt nanowires possess fewer undesirable low coordination sites that results in their improved catalytic activity. Additionally, we believe that sulfur with 1.40 at% is an ideal amount in SG to achieve uniform Pt nanowire morphology and geometry leading to a higher ECSA, activity and stability of PtNW/SG-2. Based on measurement of over 50 individual nanowires, the nanowires supported by SG-2 are smaller than the nanowires supported by G and SG-1 and notably, the growth of nanowires was significantly interrupted onto SG-3 and SG-4. The presence of a high amount of sulfur in SG-3 and SG-4 might provide too many anchoring sites where nanoparticles nucleate and begin to elongate, leaving insufficient platinum precursors in solution to continue the formation of well-defined, smooth nanowires. However, the ORR activity of G and various SG (Figure S13 in Supporting information) show that G, SG-2 and SG-4 have minimal ORR activity in acidic media.

Mass transport corrected Tafel plots at different temperatures for PtNW/G and PtNW/SG catalysts are shown in Figure 6a-d. At any temperature, the low and the high Tafel slopes can be determined for each catalyst and correspond to the potential regime where oxygen reduction proceeds on oxide-covered Pt surface (Temkin conditions) and on oxide-free Pt surface (Langmuir conditions), respectively [49]. The low and high Tafel slopes from the logJ_k-V plots

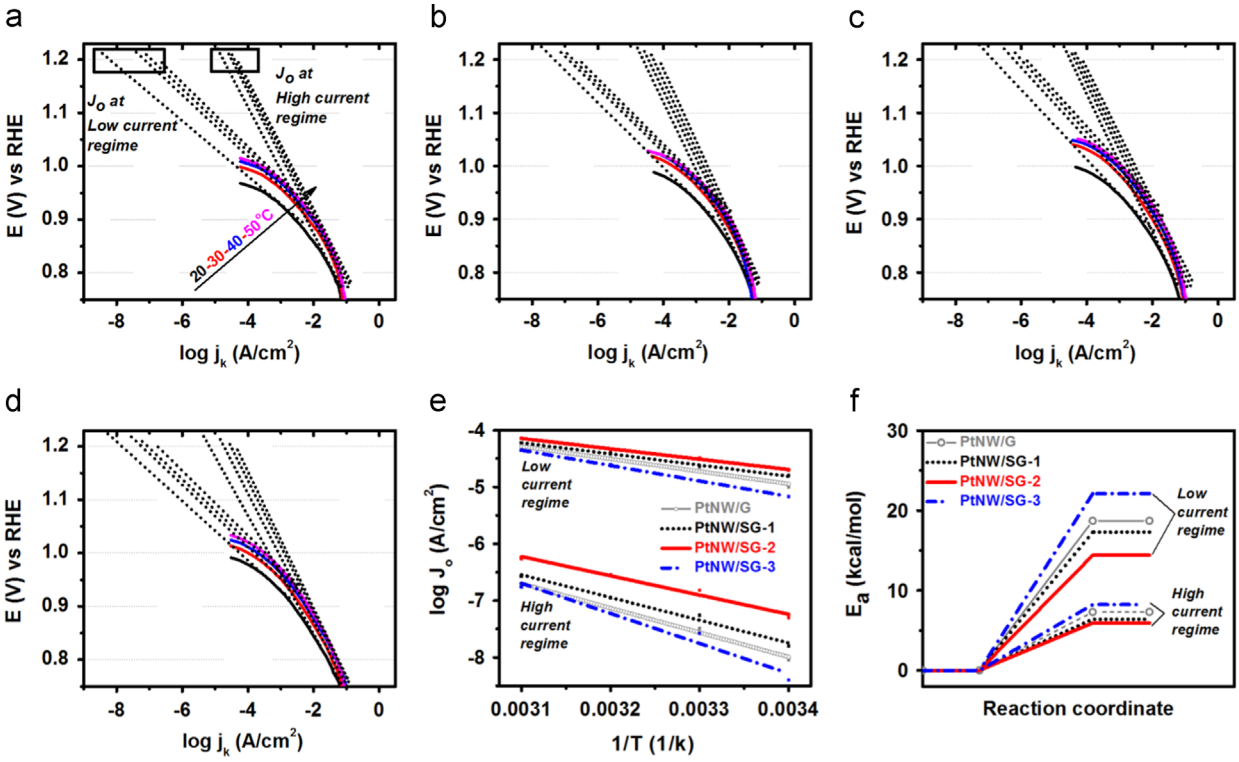

Figure 6 Mass transport corrected Tafel plots for oxygen reduction as a function of temperature obtained for (a) PtNW/G, (b) PtNW/SG-1, (c) PtNW/SG-2 and (d) PtNW/SG-3. (e) Arrhenius plots for the exchange current density for oxygen reduction corresponding to the low and high current density region of PtNW/G, PtNW/SG-1, PtNW/SG-2 and PtNW/SG-3, (f) Comparison of activation energy (E_a) of the catalysts at low and high current density region.

calculated at different temperatures for PtNW/G, PtNW/SG-1, PtNW/SG-2 and PtNW/SG-3 catalysts remain essentially constant (low Tafel slope: 60 ± 5 mV/dec and high Tafel slope: 120 ± 5 mV/dec) [77]. The exchange current density (j_0) corresponding to each Tafel slope was calculated by extrapolating the potential to the temperature corrected reversible potential (E_r), with the determined values listed in Table S2 in the Supporting information. Note that, the dependence of E_r on temperature was evaluated using the following equations [49]:

$$\Delta G^0 = -70650 - 8.0T \ln T + 92.84\,T$$

$$E_r = -\Delta G^0/nF$$

where ΔG^0 is the free energy for O_2-H_2 reaction producing liquid water, n is the number of electrons transferred to produce one mole of water, $n=2$ and F is Faraday's constant, 96485 coulombs.

The temperature dependence exchange current densities in both Tafel regimes for each catalyst were plotted in Figure 6e, and the activation energy for oxygen reduction of the catalyst was determined using the following Arrhenius equation.

$$E_a = -2.303R\left[d \log j_k / d(1/T)\right]$$

where E_a is the activation energy in kcal/mole, R is the gas constant with a value of 8.31 J/molK and T is the temperature in K. Figure 6f shows the apparent activation energy diagram of various catalysts in both low and high current density regimes. The activation energy calculated for PtNW/G, PtNW/SG-1, PtNW/SG-2 and PtNW/SG-3 were 18.7, 17.3, 14.4, 22.1 kcal/mol in low current density regime (at 0.95 V) and 7.31, 6.40, 5.94 and 8.23 kcal/mol in high current density regime (at 0.85 V), respectively. These values are in close agreement with values reported in the literature for both the high current density regime [49] and the low current density regime [78,79]. It should be noted that PtNW/SG-4 was omitted from temperature dependent studies owing to its relatively poor ORR performance in comparison to other catalysts. Interestingly, PtNW/SG-2 possesses significantly higher exchange current density and lower activation energy on both oxide-covered and oxide-free surfaces in comparison to other catalysts. This again demonstrates the high electrocatalytic activity of this catalyst towards the ORR. In an O_2-reduction reaction, it was shown experimentally and theoretically that the first electron transfer ($O_2 + H^+ + e^- \rightarrow O_2H_{ads}$) is the rate determining step if the difference between the activation energies on oxide-covered and oxide-free Pt surface is 4 kcal/mol [80]. However, in our studies, the difference between the activation energies of each catalyst was above 8 kcal/mol, which might indicate the existence of a chemical step [3] following the first electron-transfer on the Pt surface [50,80]. Therefore, the following reaction mechanism can be considered to elucidate the catalytic properties of various catalyst materials:

$$2Pt\ldots O_2 \leftrightarrow Pt_2O_{2ads}$$

$$Pt_2O_{2ads} + H^+ + e^- \leftrightarrow Pt_2O_2H_{ads} \text{ (first electron-transfer step)}$$

$$Pt_2O_2H_{ads} \rightarrow Pt\text{-}O + Pt\text{-}OH \text{ (chemical step)}$$

$$Pt\text{-}O + Pt\text{-}OH + H^+ + e^- \rightarrow Pt\text{-}OH + Pt\text{-}OH$$

$$Pt\text{-}OH + Pt\text{-}OH + 2H^+ + 2e^- \rightarrow 2Pt + 2H_2O$$

While considering the reaction steps mentioned above, the fractional coverage of reaction intermediates in the rate determining step can be significantly reduced for PtNW/SG-2 due to its high exchange current density and low activation energy compare to other catalysts. This can be attributed to a weak binding between oxygenated species and the Pt surface atoms which is beneficial for enhancing ORR kinetics. Therefore, it is obvious that the amount of sulfur in graphene is a crucial parameter to tune the electrokinetics of nanowire catalysts. It is now demonstrated that 1.40 at% of sulfur in graphene provides improved physico-chemical properties favorable to enhance Pt electrocatalytic activity and stability. To illustrate, based on our DFT analysis on various SG materials shown in Figure S14 (see Supporting information), it can be established that for SG with 0.35 at% sulfur (SG-1), the DOS of SG is almost equal to that of pristine graphene, showing a Dirac point which has no band gap and energy of states supposes to display a similar ORR activity in comparison with that on pure graphene. Interestingly, the performance observed was similar for both G and SG-1 supported PtNWs. On the other hand, at higher sulfur contents, the physico-chemical properties of SG-3 (2.70 at% of sulfur) and SG-4 (3.95 at% of sulfur) were adversely affected leading to an interruption on the growth of well-defined PtNWs that can potentially result in the reduced ORR activity and stability.

Conclusions

Through experimental and computational investigations, we provide detail fundamental insight for designing PtNW/SGs as ORR catalysts in acidic electrolyte. A series of SG materials with varying sulfur contents ranging from 0.35 to 3.95 at% were prepared. We found that the amount of sulfur significantly affects the ORR kinetics of nanowire catalysts due to the influence of the sulfur dopants present in SG. With increasing sulfur contents, the number of graphene layers increased as determined by XRD. Furthermore, the ratio of SP^2 and SP^3 carbon decreases, indicating a less graphitic character of SG. Moreover, the results obtained from UV-vis and LPR technique show that the band gap increases and the electrical conductivity decreases with increasing the amount of sulfur in graphene matrix and these results are well consistent with the results obtained from DFT analysis. PtNW/SG-2 (1.40 at% sulfur) shows the best electrokinetic performance, with a mass activity of 182 mA/mg_{Pt} and a specific activity of 662 μA/cm^2_{Pt} at 0.9 V vs. RHE. Moreover, PtNW/SG-2 shows a high exchange current density and low activation energy which leads to a weakened interaction between the nonreactive oxygenated species and Pt surface atoms that is beneficial for enhancing ORR kinetics.

Acknowledgments

The work was supported by NSERC, the University of Waterloo and the Waterloo Institute for Nanotechnology. This research was conducted as part of the Catalysis Research for Polymer Electrolyte Fuel Cells (CaRPE FC) Network administered from Simon Fraser University and supported by Automotive Partnership Canada (APC) Grant

APCPJ 417858-11 through the Natural Sciences and Engineering Research Council of Canada (NSERC).

Appendix A. Supplementary material

Supplementary data associated with this article can be found in the online version at http://dx.doi.org/10.1016/j.nanoen.2015.11.004.

References

[1] D. Strmcnik, M. Escudero-Escribano, K. Kodama, V.R. Stamenkovic, A. Cuesta, N.M. Markovic, Nat. Chem. 2 (2010) 880–885.
[2] A. Holewinski, J.C. Idrobo, S. Linic, Nat. Chem. 6 (2014) 941.
[3] V.R. Stamenkovic, B. Fowler, B.S. Mun, G.F. Wang, P.N. Ross, C.A. Lucas, N.M. Markovic, Science 315 (2007) 493–497.
[4] C. Wang, N.M. Markovic, V.R. Stamenkovic, ACS Catal. 2 (2012) 891–898.
[5] D. Zhao, B.Q. Xu, Angew. Chem. 118 (2006) 5077–5081.
[6] A.A. Topalov, I. Katsounaros, M. Auinger, S. Cherevko, J.C. Meier, S.O. Klemm, K.J.J. Mayrhofer, Angew. Chem. Int. Ed. 51 (2012) 12613–12615.
[7] L. Tang, B. Han, K. Persson, C. Friesen, T. He, K. Sieradzki, G. Ceder, J. Am. Chem. Soc. 132 (2010) 596–600.
[8] X.W. Yu, S.Y. Ye, J. Power Sources 172 (2007) 145–154.
[9] C. Koenigsmann, A.C. Santulli, K.P. Gong, M.B. Vukmirovic, W.P. Zhou, E. Sutter, S.S. Wong, R.R. Adzic, J. Am. Chem. Soc. 133 (2011) 9783–9795.
[10] N.M. Markovic, T.J. Schmidt, V. Stamenkovic, P.N. Ross, Fuel Cells 1 (2001) 105–116.
[11] L.J. Yang, M.B. Vukmirovic, D. Su, K. Sasaki, J.A. Herron, M. Mavrikakis, S.J. Liao, R.R. Adzic, J. Phys. C.hem. C. 117 (2013) 1748–1753.
[12] A. Holewinski, S. Linic, J. Electrochem. Soc. 159 (2012) H864–H870.
[13] S.H. Sun, G.X. Zhang, D.S. Geng, Y.G. Chen, R.Y. Li, M. Cai, X.L. Sun, Angew. Chem. Int. Ed. 50 (2011) 422–426.
[14] J.X. Chen, J.B. Siegel, T. Matsuura, A.G. Stefanopoulou J. Electrochem. Soc. 158 (2011) B1164–B1174.
[15] R.Y. Wang, C.X. Xu, X.X. Bi, Y. Ding, Energy Environ. Sci. 5 (2012) 5281–5286.
[16] S.J. Guo, D.G. Li, H.Y. Zhu, S. Zhang, N.M. Markovic, V.R. Stamenkovic, S.H. Sun, Angew. Chem. Int. Ed. 52 (2013) 3465–3468.
[17] Z.W. Chen, M. Waje, W.Z. Li, Y.S. Yan, Angew. Chem. Int. Ed. 46 (2007) 4060–4063.
[18] S.J. Guo, S. Zhang, D. Su, S.H. Sun, J. Am. Chem. Soc. 135 (2013) 13879–13884.
[19] D.C. Higgins, R.Y. Wang, M.A. Hoque, P. Zamani, S. Abureden, Z.W. Chen, Nano Energy 10 (2014) 135–143.
[20] R. Wang, D.C. Higgins, M.A. Hoque, D. Lee, F. Hassan, Z. Chen, Sci. Rep. 3 (2013) 2431.
[21] D.C. Higgins, S.Y. Ye, S. Knights, Z.W. Chen, Electrochem. Solid State Lett. 15 (2012) B83–B85.
[22] B.Y. Xia, H.B. Wu, Y. Yan, X.W. Lou, X. Wang, J. Am. Chem. Soc. 135 (2013) 9480–9485.
[23] H.W. Liang, X.A. Cao, F. Zhou, C.H. Cui, W.J. Zhang, S.H. Yu, Adv. Mater. 23 (2011) 1467–1471.
[24] C. Koenigsmann, S.S. Wong, Energy Environ. Sci. 4 (2011) 1161–1176.
[25] Y.N. Xia, P.D. Yang, Y.G. Sun, Y.Y. Wu, B. Mayers, B. Gates, Y.D. Yin, F. Kim, Y.Q. Yan, Adv. Mater. 15 (2003) 353–389.
[26] L. Cademartiri, G.A. Ozin, Adv. Mater. 21 (2009) 1013–1020.
[27] Y.Y. Shao, G.P. Yin, Y.Z. Gao, J. Power Sources 171 (2007) 558–566.
[28] C. Wang, M. Waje, X. Wang, J.M. Tang, R.C. Haddon, Y.S. Yan, Nano Lett. 4 (2004) 345–348.
[29] S.H. Sun, F. Jaouen, J.P. Dodelet, Adv. Mater. 20 (2008) 3900.
[30] S.H. Sun, G.X. Zhang, D.S. Geng, Y.G. Chen, M.N. Banis, R.Y. Li, M. Cai, X.L. Sun, Chem. – Eur. J. 16 (2010) 829–835.
[31] S.H. Sun, G.X. Zhang, Y. Zhong, H. Liu, R.Y. Li, X.R. Zhou, X.L. Sun, Chem. Commun. (2009) 7048–7050.
[32] D. Higgins, M.A. Hoque, M.H. Seo, R. Wang, F. Hassan, J.-Y. Choi, M. Pritzker, A. Yu, J. Zhang, Z. Chen, Adv. Funct. Mater. 24 (2014) 4325–4336.
[33] M.A. Hoque, F.M. Hassan, D. Higgins, J.Y. Choi, M. Pritzker, S. Knights, S. Ye, Z. Chen, Adv. Mater. 27 (2015) 1229–1234.
[34] M.A. Hogue, D.C. Higgins, F.M. Hassan, J.Y. Choi, M.D. Pritzker, Z.W. Chen, Electrochim. Acta 121 (2014) 421–427.
[35] Y. Jiang, J. Zhang, Y.H. Qin, D.F. Niu, X.S. Zhang, L. Niu, X.G. Zhou, T.H. Lu, W.K. Yuan, J. Power Sources 196 (2011) 9356–9360.
[36] J.E. Park, Y.J. Jang, Y.J. Kim, M.S. Song, S. Yoon, D.H. Kim, S.J. Kim, Phys. Chem. Chem. Phys. 16 (2014) 103–109.
[37] M.M. Liu, R.Z. Zhang, W. Chen, Chem. Rev. 114 (2014) 5117–5160.
[38] V. Chabot, D. Higgins, A.P. Yu, X.C. Xiao, Z.W. Chen, J.J. Zhang, Energy Environ. Sci. 7 (2014) 1564–1596.
[39] H.T. Liu, Y.Q. Liu, D.B. Zhu, J. Mater. Chem. 21 (2011) 3335–3345.
[40] D.W. Kim, O.L. Li, N. Saito, Phys. Chem. Chem Phys. 17 (2015) 407–413.
[41] Z.L. Ma, S. Dou, A.L. Shen, L. Tao, L.M. Dai, S.Y. Wang, Angew. Chem. Int. Ed. 54 (2015) 1888–1892.
[42] K.P. Gong, F. Du, Z.H. Xia, M. Durstock, L.M. Dai, Science 323 (2009) 760–764.
[43] D.S. Yu, Q. Zhang, L.M. Dai, J. Am. Chem. Soc. 132 (2010) 15127–15129.
[44] Y. Li, Y. Zhao, H.H. Cheng, Y. Hu, G.Q. Shi, L.M. Dai, L.T. Qu, J. Am. Chem. Soc. 134 (2012) 15–18.
[45] C.H. Hsu, J.Y. Jan, H.P. Lin, P.L. Kuo, New. J. Chem. 38 (2014) 5521–5526.
[46] R.I. Jafri, N. Rajalakshmi, S. Ramaprabhu, J. Mater. Chem. 20 (2010) 7114–7117.
[47] D.C. Marcano, D.V. Kosynkin, J.M. Berlin, A. Sinitskii, Z.Z. Sun, A. Slesarev, L.B. Alemany, W. Lu, J.M. Tour, ACS Nano 4 (2010) 4806–4814.
[48] S.H. Park, S.M. Bak, K.H. Kim, J.P. Jegal, S.I. Lee, J. Lee, K. B. Kim, J. Mater. Chem. 21 (2011) 680–686.
[49] A. Parthasarathy, S. Srinivasan, A.J. Appleby, C.R. Martin, J. Electrochem. Soc. 139 (1992) 2530–2537.
[50] A. Parthasarathy, C.R. Martin, S. Srinivasan, J. Electrochem. Soc. 138 (1991) 916–921.
[51] D. van der Vliet, D.S. Strmcnik, C. Wang, V.R. Stamenkovic, N.M. Markovic, M.T.M. Koper, J. Electroanal. Chem. 647 (2010) 29–34.
[52] X.H. Yang, J.W. Guo, S. Yang, Y. Hou, B. Zhang, H.G. Yang, J. Mater. Chem. A 2 (2014) 614–619.
[53] J.M. Gonzalez-Dominguez, P. Castell, S. Bespin-Gascon, A. Anson-Casaos, A.M. Diez-Pascual, M.A. Gomez-Fatou, A.M. Benito, W.K. Maser, M.T. Martinez, J. Mater. Chem. 22 (2012) 21285–21297.
[54] F. Guzman, M. Favre, H.M. Ruiz, S. Hevia, L.S. Caballero, E.S. Wyndham, H. Bhuyan, M. Flores, S. Mandl, J. Phys. D. Appl. Phys. 46 (2013) 215202.
[55] W.S. Tseng, C.Y. Tseng, C.T. Kuo, Nanoscale Res. Lett. 4 (2009) 234–239.
[56] Z. Chen, D. Higgins, Z.W. Chen, Carbon 48 (2010) 3057–3065.
[57] Z. Chen, D. Higgins, H.S. Tao, R.S. Hsu, Z.W. Chen, J. Phys. Chem. C 113 (2009) 21008–21013.
[58] Z. Yang, Z. Yao, G.F. Li, G.Y. Fang, H.G. Nie, Z. Liu, X.M. Zhou, X. Chen, S.M. Huang, ACS Nano 6 (2012) 205–211.

[59] F.M. Hassan, V. Chabot, J.D. Li, B.K. Kim, L. Ricardez-Sandoval, A.P. Yu, J. Mater. Chem. A 1 (2013) 2904–2912.
[60] B.K. Saikia, R.K. Boruah, P.K. Gogoi, J. Chem. Sci. 121 (2009) 103–106.
[61] C.F. Yuan, W.F. Chen, L.F. Yan, J. Mater. Chem. 22 (2012) 7456–7460.
[62] J. Tauc, R. Grigorov., A. Vancu, Phys. Status Solidi 15 (1966) 627–637.
[63] J. Tauc, Science 158 (1967) 1543–1548.
[64] L. Ci, L. Song, C.H. Jin, D. Jariwala, D.X. Wu, Y.J. Li, A. Srivastava, Z.F. Wang, K. Storr, L. Balicas, F. Liu, P.M. Ajayan, Nat. Mater. 9 (2010) 430–435.
[65] A. Mathkar, D. Tozier, P. Cox, P.J. Ong, C. Galande, K. Balakrishnan, A.L.M. Reddy, P.M. Ajayan, J. Phys. Chem. Lett. 3 (2012) 986–991.
[66] S. Stankovich, D.A. Dikin, R.D. Piner, K.A. Kohlhaas, A. Kleinhammes, Y. Jia, Y. Wu, S.T. Nguyen, R.S. Ruoff, Carbon 45 (2007) 1558–1565.
[67] Y.G. Chen, J.J. Wang, X.B. Meng, Y. Zhong, R.Y. Li, X.L. Sun, S.Y. Ye, S. Knights, Int. J. Hydrog. Energy 36 (2011) 11085–11092.
[68] D.C. Higgins, D. Meza, Z.W. Chen, J. Phys. Chem. C 114 (2010) 21982–21988.
[69] L.Y. Ruan, E.B. Zhu, Y. Chen, Z.Y. Lin, X.Q. Huang, X.F. Duan, Y. Huang, Angew. Chem. Int. Ed. 52 (2013) 12577–12581.
[70] Y.J. Li, Y.J. Li, E.B. Zhu, T. McLouth, C.Y. Chiu, X.Q. Huang, Y. Huang, J. Am. Chem. Soc. 134 (2012) 12326–12329.
[71] B. Lim, M.J. Jiang, P.H.C. Camargo, E.C. Cho, J. Tao, X.M. Lu, Y.M. Zhu, Y.N. Xia, Science 324 (2009) 1302–1305.
[72] I.E.L. Stephens, A.S. Bondarenko, F.J. Perez-Alonso, F. Calle-Vallejo, L. Bech, T.P. Johansson, A.K. Jepsen, R. Frydendal, B. P. Knudsen, J. Rossmeisl, I. Chorkendorff, J. Am. Chem. Soc. 133 (2011) 5485–5491.
[73] V.R. Stamenkovic, B.S. Mun, K.J.J. Mayrhofer, P.N. Ross, N.M. Markovic, J. Am. Chem. Soc. 128 (2006) 8813–8819.
[74] J. Greeley, I.E.L. Stephens, A.S. Bondarenko, T.P. Johansson, H.A. Hansen, T.F. Jaramillo, J. Rossmeisl, I. Chorkendorff, J.K. Norskov, Nat. Chem. 1 (2009) 552–556.
[75] J.L. Zhang, M.B. Vukmirovic, Y. Xu, M. Mavrikakis, R.R. Adzic, Angew. Chem. Int. Ed. 44 (2005) 2132–2135.
[76] J.K. Norskov, J. Rossmeisl, A. Logadottir, L. Lindqvist, J.R. Kitchin, T. Bligaard, H. Jonsson, J. Phys. Chem. B 108 (2004) 17886–17892.
[77] W.E. Ogrady, E.J. Taylor, S. Srinivasan, J. Electroanal. Chem. 132 (1982) 137–150.
[78] U.A. Paulus, A. Wokaun, G.G. Scherer, T.J. Schmidt, V. Stamenkovic, V. Radmilovic, N.M. Markovic, P.N. Ross, J. Phys. Chem. B 106 (2002) 4181–4191.
[79] J.P. Perdew, K. Burke, M. Ernzerhof, Phys. Rev. Lett. 77 (1996) 3865–3868.
[80] D.B. Sepa, M.V. Vojnovic, L.M. Vracar, A. Damjanovic, Electrochim. Acta 29 (1984) 1169–1170.

Md. Ariful Hoque is currently doing his Ph.D. in Chemical Engineering at the University of Waterloo, Canada. He obtained his MASc in Chemical Engineering from Yeungnam University, South Korea and B.Sc. in Chemical Engineering from Bangladesh University of Engineering and Technology (BUET), Bangladesh. His research focuses on the development of heteroatom-doped carbon nanostructures as platinum supports for fuel cell applications.

Dr. Fathy M. Hassan obtained his Ph.D. in Physical Chemistry from Cairo University in 2004. He held the Japan Society for Promotion of Science Award for foreign scientists at the National Institute of Advanced Industrial Science and Technology. He obtained his second Ph.D. in Chemical Engineering (Nanotechnology) from University of Waterloo in 2014. He obtained the honored award of outstanding achievements and Park and Veva Reilly Medal for Proficiency in Research at University of Waterloo. Currently, he is a postdoctoral fellow with research interests spanning the area of synthetic materials chemistry and nano-architecture materials for advanced electrochemical energy storage and conversion devices.

Min Ho Seo received his Bachelor's degree in Advanced Materials Science and Engineering from Sungkyunkwan University in 2005, Master's degree and Ph.D. in Materials Science from Gwangju Institute of Science and Technology in 2007 and 2012 under the supervision of Prof. Won Bae Kim. He is currently a postdoctoral fellow working with Prof. Zhongwei Chen at the University of Waterloo. His current research is mainly focused on the catalyst development based on novel support materials and non-precious catalysts for fuel-cell and metal-air battery applications through both experimental and the first principle studies (DFT).

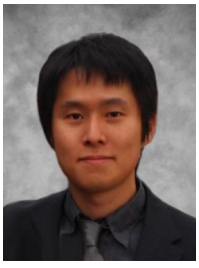

Ja-Yeon Choi is a Ph.D. student in Chemical Engineering at the University of Waterloo in Dr. Zhongwei Chen's research group, and a visiting researcher at Ballard Power Systems. He completed his Masters in 2013 on the application of nanostructured carbon materials and novel precursors to develop non-precious metal catalysts for Proton Exchange Membrane fuel cells. His current research interests lie in the development of advanced nonprecious metal and Pt catalysts with controlled nanostructures for fuel cell and battery applications.

Mark Pritzker is Professor of Chemical Engineering at the University of Waterloo, Waterloo, Canada where he has been a faculty member since 1989. Dr. Pritzker's research is broadly concerned with a number of topics related to electrochemical engineering, with particular focus on the electrodeposition of thin metal and alloy films, polymer electrolyte and solid-oxide fuel cells, lithium battery design and modeling and nanotechnology. He is an active member of the Canadian Society for Chemical Engineers, American Institute of Chemical Engineers and the Electrochemical Society.

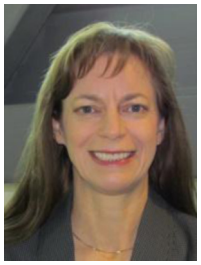

Ms. Shanna Knights is Director of Research at Ballard Power Systems. Her fuel cell research areas since joining Ballard in 1995 include durability, reliability, performance, and operational behavior, and span several fuel cell applications, including stationary power generation, cogeneration, bus, light duty automotive, back-up power, and materials handling. She is responsible for both internal research activities and significant collaboration with universities, research institutions and industry.

Dr. Siyu Ye is a Principal Research Scientist at Ballard Power Systems and an Adjunct Professor at the University of British Columbia, Canada. Dr. Ye received his B.Sc. in 1982 and his Ph.D. in 1988, both from Xiamen University, respectively. From 1994 to 2000, he was a senior research scientist at the Hydro-Québec Research Institute, Canada, until he joined Ballard Power Systems in 2000. Dr. Ye presently leads the Advanced Catalyst Layer Development activities within Ballard's R&D function as well as the management of several Ballard's research collaboration projects with university professors and national lab researchers in Canada and US.

Prof. Zhongwei Chen is Canada Research Chair in Advanced Materials for Clean Energy at University of Waterloo. His research interests are in the development of advanced energy materials for metal-air batteries, lithium-ion batteries and fuel cells. He was promoted to an Associate Professor with early tenure in 2012 and he was awarded Canada Research Chair in 2014. He has published 1 book, 6 book chapters and more than 130 peer reviewed journal articles with over 10,000 citations with H-index 43 (*Google Scholar*). He is also listed as inventor on 15 US/international patents, with several licensed to companies in USA and Canada.